

# Detection and Characterization of Mononuclear Pd(I) Complexes Supported by N2S2 and N4 Tetradentate Ligands

Jia Luo, Giang N. Tran, Nigam P. Rath, and Liviu M. Mirica\*

Cite This: *Inorg. Chem.* 2020, 59, 15659–15669

Read Online

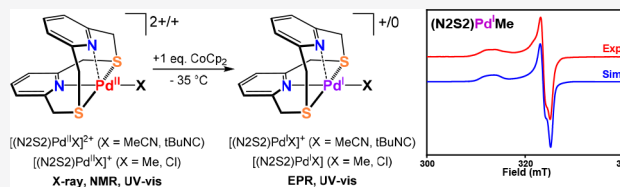
ACCESS |

Metrics & More

Article Recommendations

Supporting Information

**ABSTRACT:** Palladium is a versatile transition metal used to catalyze a large number of chemical transformations, largely due to its ability to access various oxidation states (0, I, II, III, and IV). Among these oxidation states, Pd(I) is arguably the least studied, and while dinuclear Pd(I) complexes are more common, mononuclear Pd(I) species are very rare. Reported herein are spectroscopic studies of a series of Pd(I) intermediates generated by the chemical reduction at low temperatures of Pd(II) precursors supported by the tetradentate ligands 2,11-dithia[3.3](2,6)pyridinophane (N2S2) and *N,N'*-di-*tert*-butyl-2,11-diaza[3.3](2,6)pyridinophane (<sup>t</sup>BuN4): [(N2S2)Pd<sup>II</sup>(MeCN)]<sub>2</sub>(OTf)<sub>4</sub> (1), [(N2S2)Pd<sup>II</sup>Me]<sub>2</sub>(OTf)<sub>2</sub> (2), [(N2S2)Pd<sup>II</sup>Cl](OTf) (3), [(N2S2)Pd<sup>II</sup>X](OTf)<sub>2</sub> (X = *t*BuNC 4, PPh<sub>3</sub> 5), [(N2S2)Pd<sup>II</sup>Me(PPh<sub>3</sub>)](OTf) (6), and [(<sup>t</sup>BuN4)Pd<sup>II</sup>X<sub>2</sub>](OTf)<sub>2</sub> (X = MeCN 8, *t*BuNC 9). In addition, a stable Pd(I) dinuclear species, [(N2S2)Pd<sup>I</sup>(μ-*t*BuNC)]<sub>2</sub>(ClO<sub>4</sub>)<sub>2</sub> (7), was isolated upon the electrochemical reduction of 4 and structurally characterized. Moreover, the (<sup>t</sup>BuN4)Pd<sup>I</sup> intermediates, formed from the chemical reduction of [(<sup>t</sup>BuN4)Pd<sup>II</sup>X<sub>2</sub>](OTf)<sub>2</sub> (X = MeCN 8, *t*BuNC 9) complexes, were investigated by EPR spectroscopy, X-ray absorption spectroscopy (XAS), and DFT calculations and compared with the analogous (N2S2)Pd<sup>I</sup> systems. Upon probing the stability of Pd(I) species under different ligand environments, it is apparent that the presence of soft ligands such as *t*BuNC and PPh<sub>3</sub> significantly improves the stability of Pd(I) species, which should make the isolation of mononuclear Pd(I) species possible.



## INTRODUCTION

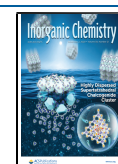
Palladium is a versatile transition metal used to catalyze a large number of chemical transformations, largely due to its ability to access various oxidation states (0, I, II, III, and IV). The Pd(0) and Pd(II) systems are by far the most extensively studied for catalytic applications,<sup>1,2</sup> and the chemistry of high-valent Pd(III) and Pd(IV) complexes has also received significant attention in the past few years.<sup>3–11</sup> By comparison, the reports describing Pd(I) complexes are far less, although Pd(I) species have been proposed to play important roles in radical atom transfer and cross-coupling reactions.<sup>12–22</sup> While several reports describe the detection of transient mononuclear Pd(I) species,<sup>23–28</sup> only one structurally characterized mononuclear Pd(I) cationic species [Pd<sup>I</sup>(*t*Bu<sub>3</sub>P)<sub>2</sub>]<sup>+</sup> has been reported independently by two research groups;<sup>29,30</sup> however, no further reactivity studies were reported for this complex, even though it decomposes in solution at room temperature. An earlier report also described an isolated mononuclear Pd(I) complex, although the presence of a redox noninnocent ligand complicates the unambiguous Pd center oxidation state assignment.<sup>31</sup> In addition, most of the isolated Pd(I) complexes reported to date are dinuclear Pd(I) species containing a Pd(I)–Pd(I) bond and thus are closed-shell systems.

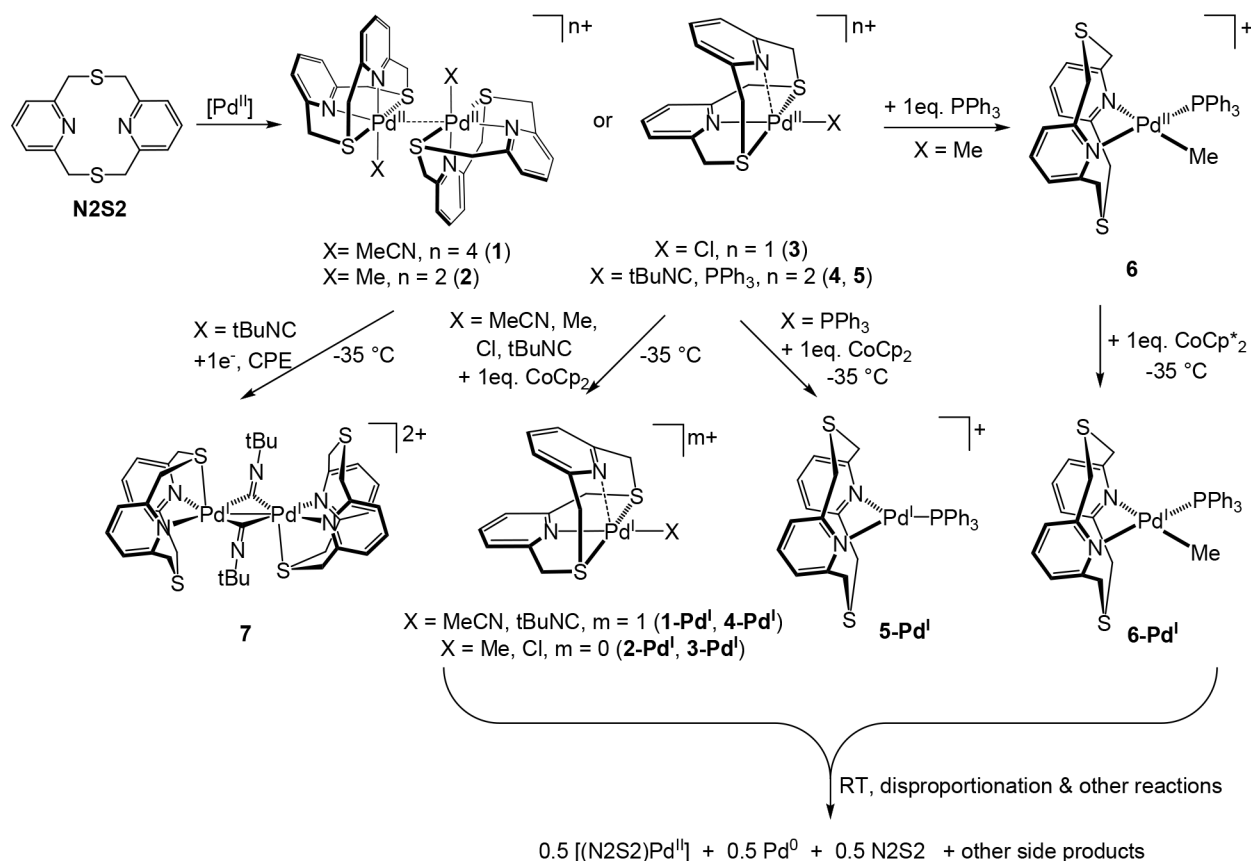
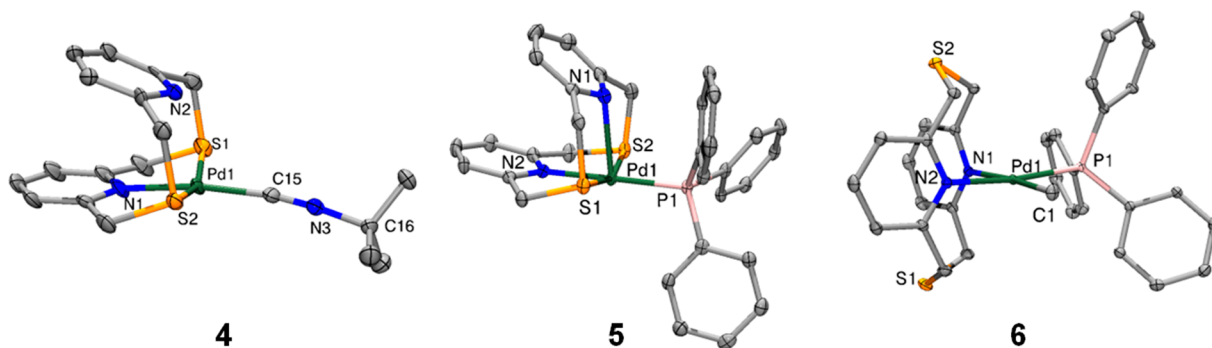
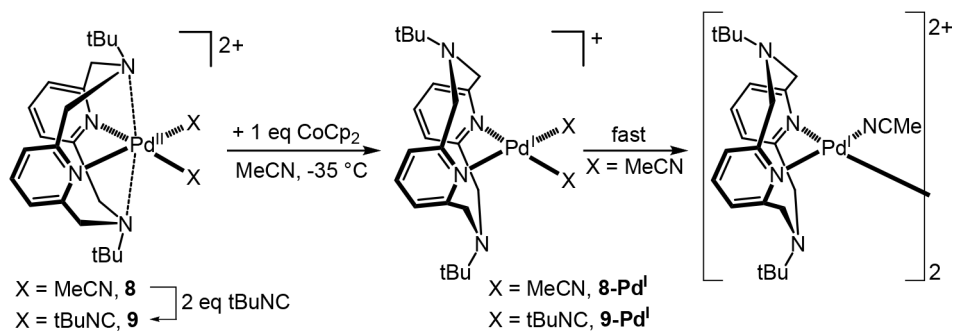
Given our long-term interest in developing catalytic transformations employing odd-electron Pd(I) and Pd(III) species,<sup>32–38</sup> we are actively targeting the synthesis and

investigation of mononuclear Pd(I) complexes. In this regard, reported herein are spectroscopic studies of a series of Pd(I) intermediates generated by the chemical reduction of Pd(II) precursors supported by the tetradentate ligands 2,11-dithia[3.3](2,6)pyridinophane (N2S2) and *N,N'*-di-*tert*-butyl-2,11-diaza[3.3](2,6)pyridinophane (<sup>t</sup>BuN4): [(N2S2)Pd<sup>II</sup>(MeCN)]<sub>2</sub>(OTf)<sub>4</sub> (1), [(N2S2)Pd<sup>II</sup>Me]<sub>2</sub>(OTf)<sub>2</sub> (2), [(N2S2)Pd<sup>II</sup>Cl](OTf) (3), [(N2S2)Pd<sup>II</sup>X](OTf)<sub>2</sub> (X = *t*BuNC 4, PPh<sub>3</sub> 5), [(N2S2)Pd<sup>II</sup>Me(PPh<sub>3</sub>)](OTf) (6), and [(<sup>t</sup>BuN4)Pd<sup>II</sup>X<sub>2</sub>](OTf)<sub>2</sub> (X = MeCN 8, *t*BuNC 9, Scheme 1). In addition, a stable Pd(I) dinuclear species, [(N2S2)Pd<sup>I</sup>(μ-*t*BuNC)]<sub>2</sub>(ClO<sub>4</sub>)<sub>2</sub> (7), was isolated upon the electrochemical reduction of 4. Moreover, the (<sup>t</sup>BuN4)Pd<sup>I</sup> intermediates, formed from the chemical reduction of [(<sup>t</sup>BuN4)Pd<sup>II</sup>X<sub>2</sub>](OTf)<sub>2</sub> (X = MeCN 8, *t*BuNC 9, Scheme 2) complexes, were investigated by EPR spectroscopy, X-ray absorption spectroscopy (XAS), and DFT calculations and compared with the analogous (N2S2)Pd<sup>I</sup> systems. Upon probing the stability of Pd(I) species under various ligand environments (N2S2 and

Received: June 30, 2020

Published: October 15, 2020



Scheme 1. Synthesis of (N2S2)Pd<sup>II</sup> and (N2S2)Pd<sup>I</sup> Complexes and Proposed DecompositionScheme 2. Synthesis of (tBu<sup>4</sup>N4)Pd<sup>II</sup> and (tBu<sup>4</sup>N4)Pd<sup>I</sup> Complexes and Proposed Dimerization of 8 in Solution

**Figure 1.** ORTEP representations of the dications of 4, 5, and 6, shown with 50% thermal ellipsoids and with the triflate counteranions and H atoms omitted for clarity. Selected bond distances (Å) for 4: Pd1–C15 1.935(9), Pd1–S1 2.349(3), Pd1–S2 2.336(2), Pd1–N1 2.041(7), Pd1...N2 2.573(7), N3–C15 1.157(10); for 5: Pd1–P1 2.2670(9), Pd1–S1 2.3256(9), Pd1–S2 2.3344(9), Pd1–N2 2.082(3), Pd1–N1 2.459(3); and for 6: Pd1–N1 2.1662(14), Pd1–N2 2.1492(13), Pd1–C1 2.0466(15), Pd1–P1 2.2495(4).

<sup>t</sup>BuN<sub>4</sub>), it is apparent that the presence of soft ligands such as <sup>t</sup>BuNC and PPh<sub>3</sub> significantly improves the stability of Pd(I) species, which should make the isolation of mononuclear Pd(I) species possible.

## RESULTS AND DISCUSSION

### Synthesis and Characterization of Pd(II) Precursors.

The series of complexes [(N<sub>2</sub>S<sub>2</sub>)Pd<sup>II</sup>(MeCN)]<sub>2</sub>(OTf)<sub>4</sub> (**1**), [(N<sub>2</sub>S<sub>2</sub>)Pd<sup>II</sup>Me]<sub>2</sub>(OTf)<sub>2</sub> (**2**), and [(N<sub>2</sub>S<sub>2</sub>)Pd<sup>II</sup>Cl](OTf) (**3**) were synthesized by following the previously reported procedures.<sup>37,39</sup> The addition of 2 equiv <sup>t</sup>BuNC or PPh<sub>3</sub> to a MeCN solution of **1** generated complexes [(N<sub>2</sub>S<sub>2</sub>)Pd<sup>II</sup>(<sup>t</sup>BuNC)](OTf)<sub>2</sub> (**4**) and [(N<sub>2</sub>S<sub>2</sub>)Pd<sup>II</sup>(PPh<sub>3</sub>)](OTf)<sub>2</sub> (**5**) complexes, respectively, which were isolated as red crystals (Scheme 1). The X-ray crystal structures of **4** and **5** reveal that Pd(II) centers are in a distorted square pyramidal geometry with both <sup>t</sup>BuNC and PPh<sub>3</sub> ligands replacing the MeCN molecule in the equatorial position, while the N<sub>2</sub>S<sub>2</sub> ligand remains in the unusual  $\kappa^3$  conformation (Figure 1).<sup>39</sup> A significant intramolecular  $\pi$ - $\pi$  interaction between two pyridine rings was observed, with the pyridine ring centroid-centroid interplanar distance of 3.44 and 3.65 Å for **4** and **5**, respectively.<sup>40</sup> However, in contrast to the dinuclear complexes **1** and **2**, the Pd-Pd d<sup>8</sup>-d<sup>8</sup> interactions in **4** and **5** were no longer observed in the solid state, likely due to the steric effect of the <sup>t</sup>BuNC and PPh<sub>3</sub> groups. The Pd-S<sub>ave</sub> bond lengths of 2.343 Å for **4** and 2.330 Å for **5** are comparable to those of **1** and **2**, while the tilt angle of the pyridine ring vs the Pd-N<sub>ax</sub> bond in **5** of 52.8° is smaller than that in **4** of 54.9°, consistent with the shorter bond length of Pd-N<sub>ax</sub> (2.459 Å) in **5** than that of **4** (2.573 Å). Interestingly, the UV-vis spectrum of a freshly prepared MeCN solution of **5** (0.9 mM) exhibits an absorption band at 503 nm, which slowly decays over the course of several hours (Figure 2), and a diluted solution of **5**

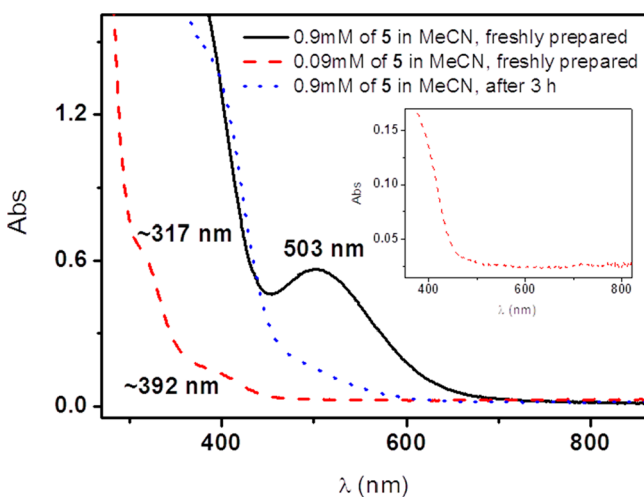


**Figure 2.** UV-vis spectra of **5** in MeCN. Inset: zoomed-in UV-vis spectrum in the 400–800 nm range for a freshly prepared 0.09 mM MeCN solution of **5**.

(0.09 mM) does not exhibit the 503 nm absorption band. The change of the UV-vis spectrum of **5** in solution suggests that the binding mode of the N<sub>2</sub>S<sub>2</sub> ligand could change from a  $\kappa^3$  conformation to a  $\kappa^2$  conformation, with the PPh<sub>3</sub> ligand and the two N donor atoms positioned in the equatorial plane, while the two S atoms are weakly interacting (or not

interacting at all) with the Pd center in the axial position. Such a conformation change process could be facilitated by the presence of a coordinating solvent, as seen previously.<sup>39</sup> The addition of PPh<sub>3</sub> to a MeCN solution of **2** gives [(N<sub>2</sub>S<sub>2</sub>)Pd<sup>II</sup>Me(PPh<sub>3</sub>)](OTf) (**6**), isolated as almost-colorless crystals. The X-ray crystal structure of **6** reveals a square-planar coordination at the Pd(II) center, with cis-positioned methyl and PPh<sub>3</sub> groups, as well as a  $\kappa^2$  conformation for N<sub>2</sub>S<sub>2</sub> (Figure 1).<sup>35,41,42</sup> The bond lengths of Pd-C (2.047 Å) and Pd-N<sub>ave</sub> (2.158 Å) are similar to (N<sub>2</sub>S<sub>2</sub>)Pd<sup>II</sup>Me<sub>2</sub>, and the Pd-P bond distance (2.250 Å) is also comparable to other reported values.<sup>43,44</sup> This conformation change of N<sub>2</sub>S<sub>2</sub> from  $\kappa^3$  to  $\kappa^2$  in the presence of PPh<sub>3</sub> in **6** further confirms the possibility of a conformational change observed in the UV-vis spectra of **5**.

**Generation and Characterization of (N<sub>2</sub>S<sub>2</sub>)Pd<sup>I</sup> Intermediates.** Cyclic voltammetry (CV) studies were performed at room temperature for the (N<sub>2</sub>S<sub>2</sub>)Pd<sup>II</sup> complexes to show that complexes **1**–**6** exhibit reduction potentials of –0.40 to –1.35 V vs Fc/Fc<sup>+</sup> in MeCN (Figures S1–S6), suggesting that the corresponding Pd(I) species should be accessible upon reduction with a chemical reductant. Therefore, these Pd(II) complexes were reacted with 1 equiv of the appropriate reducing agents in MeCN at –35 °C to generate the corresponding Pd(I) intermediates: CoCp<sub>2</sub> was used for complexes **1**–**5**, and CoCp\*<sub>2</sub> was used for **6**. Excitingly, all reaction mixtures of the reduction of complexes **1**–**6** exhibit axial or pseudoaxial signals in their EPR spectra, suggesting the presence of odd-electron species (Figure 3). Based on the simulation of the EPR data, similar superhyperfine coupling constants to the axial pyridine N atom in the g<sub>z</sub> region were detected for the [(N<sub>2</sub>S<sub>2</sub>)Pd<sup>I</sup>X]<sup>n+</sup> (X = Me **2**-Pd<sup>I</sup>, Cl **3**-Pd<sup>I</sup>, n = 0; X = MeCN **1**-Pd<sup>I</sup>, <sup>t</sup>BuNC **4**-Pd<sup>I</sup>, n = 1) complexes, suggesting a (d<sub>x<sup>2</sup>-y<sup>2</sup></sub>)<sup>1</sup> ground state for the Pd(I) centers (Figure 3 and Table 1), which should still adopt a square-pyramidal geometry with the N<sub>2</sub>S<sub>2</sub> ligand in the  $\kappa^3$  conformation. The slightly rhombic EPR spectrum of **2**-Pd<sup>I</sup> could indicate that there is a slight distortion in the equatorial plane. By comparison, the EPR spectrum of the [(N<sub>2</sub>S<sub>2</sub>)Pd<sup>I</sup>(PPh<sub>3</sub>)]<sup>+</sup> species **5**-Pd<sup>I</sup> shows no discernible superhyperfine coupling constants to the N atom(s), implying that upon reduction to Pd(I) the coordination environment has changed from square-pyramidal to a trigonal geometry, with N<sub>2</sub>S<sub>2</sub> ligand adopting a  $\kappa^2$  conformation and the two N atom donors and the P atom binding in the equatorial plane, while the two S atoms are likely no longer coordinated to the Pd center. Similarly, no superhyperfine coupling to the N or P atoms was observed for the (N<sub>2</sub>S<sub>2</sub>)Pd<sup>I</sup>Me(PPh<sub>3</sub>) species **6**-Pd<sup>I</sup>, in agreement with the  $\kappa^2$  conformation of N<sub>2</sub>S<sub>2</sub> in **6**. Overall, all observed g values are consistent with previously reported Pd(I) d<sup>9</sup> species with the g<sub>ave</sub> > 2.0023,<sup>23–28</sup> confirming that the unpaired electron resides on the Pd center rather than on the ligand(s).<sup>31</sup>

These Pd(I) complexes exhibit limited thermal stability and decompose with different rates even at low temperatures (for example, see Figure S9).<sup>45</sup> Spin integration of the EPR spectra of these Pd(I) species against a standard reveals that they form in yields from 5% to 98%, following the general trend that the presence of soft ligands such as <sup>t</sup>BuNC and Ph<sub>3</sub>P further stabilizes the Pd(I) species, while formation of dinuclear, diamagnetic Pd(I) complexes can further diminish the observed EPR signal (*vide infra*). Moreover, some of these transient Pd(I) species **1**-Pd<sup>I</sup> to **9**-Pd<sup>I</sup> seem to persist for

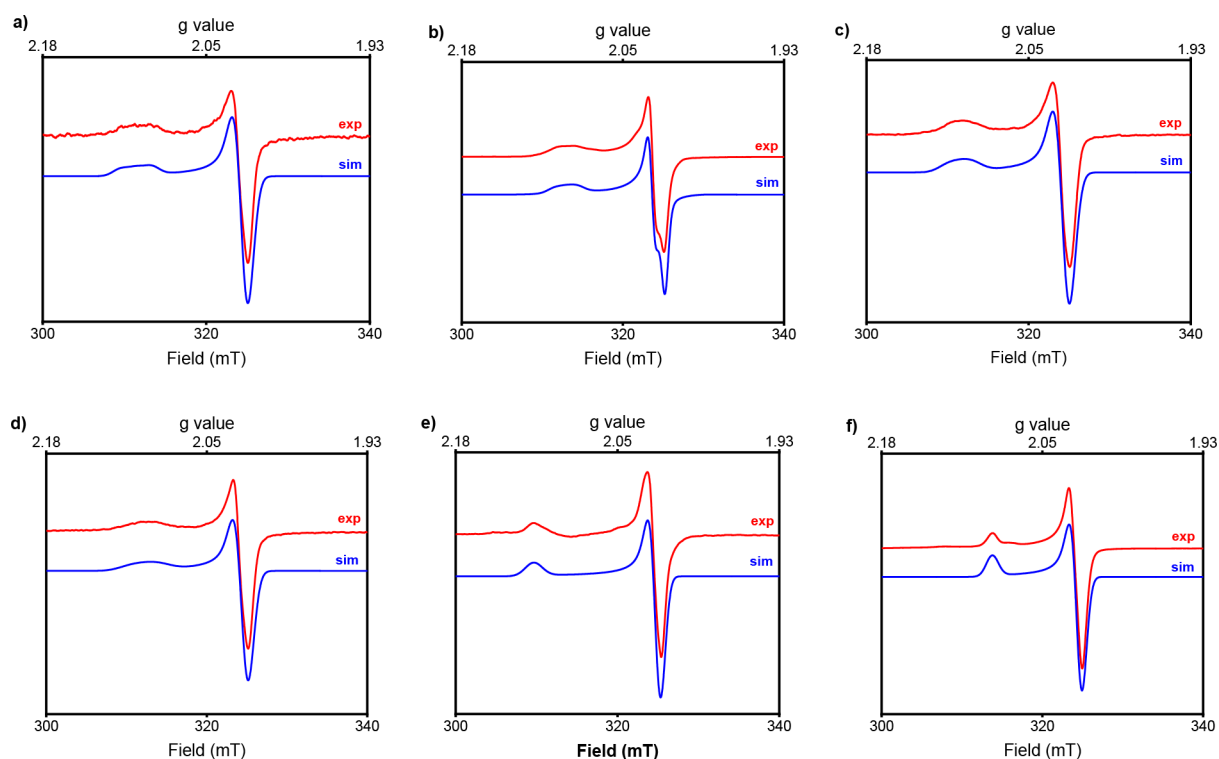


**Figure 3.** Experimental and simulated EPR spectra of reaction mixtures of  $(N_2S_2)Pd^{II}$  complexes and reducing agents at 77 K in 1:3 MeCN:PrCN frozen glass: (a–e) **1–5** +  $CoCp_2$ ; (f) **6** +  $CoCp_2^*$ .

**Table 1. Parameters Used for the Simulation of EPR Spectra of Pd(I) Species and Their Yields**

species	g values			superhyperfine coupling (G)			yield (%) <sup>b</sup>	% EPR signal left at RT after given time
	$g_x$	$g_y$	$g_z$	$A(x,x)$	$A(y,y)$	$A(z,z)$		
<b>1-Pd<sup>I</sup></b>	2.0023	2.0023	2.0870	ND <sup>a</sup>	ND	$A_{1N} = 19.0$	26	25% after 30 min
<b>2-Pd<sup>I</sup></b>	1.9983	2.0085	2.0770	ND	ND	$A_{1N} = 14.5$	80	40% after 30 min
<b>3-Pd<sup>I</sup></b>	2.0023	2.0023	2.0857	ND	ND	$A_{1N} = 16.0$	23	23% after 30 min
<b>4-Pd<sup>I</sup></b>	2.0023	2.0023	2.0820	ND	ND	$A_{1N} = 19.0$	12	11% after 1 min
<b>5-Pd<sup>I</sup></b>	1.9986	2.0023	2.0993	ND	ND	ND	90	60% after 30 min
<b>6-Pd<sup>I</sup></b>	2.0019	2.0032	2.0713	ND	ND	ND	77	20% after 5 min
<b>8-Pd<sup>I</sup></b>	1.9965	2.0063	2.0853	ND	ND	ND	5	10% after 1 min
<b>9-Pd<sup>I</sup></b>	1.9982	2.0080	2.0810	ND	ND	ND	98	25% after 5 min

<sup>a</sup>ND = not detected. <sup>b</sup>Determined by spin integration of the EPR signal against a standard.

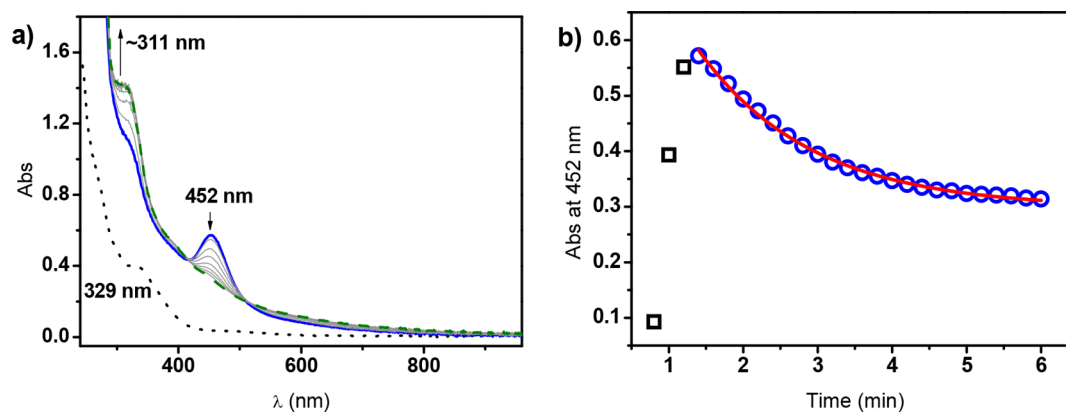


**Figure 4.** (a) UV-vis spectra of the reduction of **4** (0.12 mM, black dotted line) with 1 equiv  $CoCp_2$  in MeCN at  $-35\text{ }^\circ\text{C}$ : (thick blue solid line) spectrum at 1 min after adding  $CoCp_2$ ; (thick green dashed line) spectrum after 5 min; (thin solid lines) time interval = 0.4 min. (b) Kinetic fitting of the absorbance decay at 452 nm. Squares: 0.8–1.4 min; circles: 1.4–6 min; solid line: first-order decay fitting with the rate constant  $k = 0.656\text{ min}^{-1}$  ( $R^2 = 0.998$ ).

different lengths of time at room temperature (Table 1), lending support to our continuing efforts to isolate these Pd(I) complexes, although so far we could not crystallize these species.

To further investigate the reactivity of these Pd(I) complexes,  $^1\text{H}$  NMR was employed to monitor at room temperature the reduction of **2** and **6** by  $\text{CoCp}_2$  and  $\text{CoCp}^*_2$ , respectively (Figures S10 and S11), and to determine the nature of the final products. These results reveal that except for the formation of a small amount of  $(\text{N}_2\text{S}_2)\text{Pd}^{\text{II}}\text{Me}_2$  (<10%), likely formed upon ligand exchange,<sup>37,39</sup> the majority of the products are Pd(0) black, free N<sub>2</sub>S<sub>2</sub> ligand, and small amounts of unidentified decomposition products,<sup>45</sup> suggesting that these Pd(I) intermediates decompose by disproportionation to  $(\text{N}_2\text{S}_2)\text{Pd}(\text{II})$  species and Pd(0) and free N<sub>2</sub>S<sub>2</sub> ligand (Scheme 1) along with other ligand exchange reactions. Similar decomposition pathways have been observed previously by us for both  $(^{\text{tBu}}\text{N}_4)\text{Pd}$  and  $(\text{N}_2\text{S}_2)\text{Pd}$  systems.<sup>32–39</sup> Moreover, the only reported isolated mononuclear Pd(I) complex  $[\text{Pd}^{\text{I}}(\text{tBu}_3\text{P})_2]^+$  was also shown to undergo unidentified decomposition pathways.<sup>30</sup>

We have also monitored the chemical reduction of the  $(\text{N}_2\text{S}_2)\text{Pd}^{\text{II}}$  complexes by UV–vis spectroscopy. The UV–vis spectra of the reaction mixture of **4** and  $\text{CoCp}_2$  in MeCN at  $-35\text{ }^\circ\text{C}$  exhibit an absorption band at 452 nm (Figure 4), suggesting the formation of a Pd(I) intermediate **4-Pd<sup>I</sup>**, which was further confirmed by the corresponding EPR spectrum (Figure 3d). Both UV–vis and EPR spectra show that the corresponding signals of the **4-Pd<sup>I</sup>** species decrease within several minutes.<sup>45</sup> Monitoring of the decay of the absorbance band at 452 nm implies reveals a first-order decay process with a rate constant of  $0.656\text{ min}^{-1}$ , and this instability of the **4-Pd<sup>I</sup>** complex at  $-35\text{ }^\circ\text{C}$  prevented any isolation attempts.

Interestingly, the bulk electrolysis reduction of **4** under an inert atmosphere at room temperature yields a robust diamagnetic Pd(I) dinuclear complex  $[(\text{N}_2\text{S}_2)\text{Pd}^{\text{I}}(\mu\text{-tBuNC})_2](\text{ClO}_4)_2$  (**7**), which was isolated as orange crystals. The X-ray crystal structure of **7** shows that each Pd(I) center adopts a pseudo-square-pyramidal geometry, with one N<sub>2</sub>S<sub>2</sub> ligand binding in a  $\kappa^3$  conformation, two bridging tBuNC ligands, and one Pd(I)–Pd(I) bond: the two N donor atoms and the two tBuNC ligands define the equatorial plane, while one S donor atom weakly interacts in the axial position (Figure 5). To the best of our knowledge, there is only one other tBuNC bridged complex that has been reported to date:  $[(\text{tBuNC})_2\text{Cu}^{\text{I}}_2(\text{dppm})_2(\mu\text{-CNtBu})](\text{BF}_4)_2$ .<sup>46</sup> The bond length of CN of the bridged tBuNC group in **7** is 1.162 Å, slightly longer than the reported bridged C–N bond length (1.141 Å) in the Cu(I) complex but significantly shorter than the average bond distance of a C=N double bond (1.279 Å).<sup>47</sup> Given that this C–N bond length it is also comparable to that of the terminal tBuNC ligand in **4** (1.157 Å) and the other reported complexes with terminal tBuNC groups,<sup>48,49</sup> it suggests that the bonding interaction between the tBuNC ligand and the Pd center should not be defined as a “Pd<sup>II</sup>–(tBuNC<sup>−</sup>)” system containing a redox noninnocent tBuNC ligand. Therefore, the observed diamagnetism of **7** is likely due to the antiferromagnetic coupling between the two Pd(I) centers, with the bond distance of Pd(I)–Pd(I) (2.7416 Å) comparable to but slightly longer (0.04–0.14 Å) than other reported Pd(I)–Pd(I) bonding interactions.<sup>16,50,51</sup> While the Pd–N<sub>ave</sub> bond length is comparable to other  $(\kappa^2\text{-N}_2\text{S}_2)\text{Pd}^{\text{II}}$  complexes, the Pd–S bond (2.6588 Å) is significantly longer

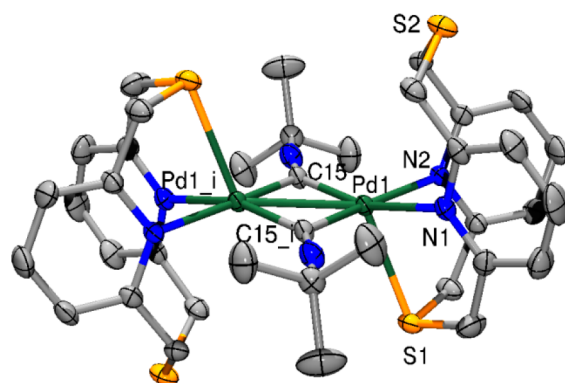


**Figure 5.** ORTEP representation of the dication in **7**, shown with 50% thermal ellipsoids and the perchlorate counteranions and H atoms omitted for clarity. Selected bond distances (Å): Pd1–N1 2.220(2), Pd1–N2 2.217(2), Pd1–C15 1.994(3), Pd1–C15<sub>i</sub> 2.076(3), Pd1–S1 2.6588(8), Pd1–Pd1<sub>i</sub> 2.7416(5), N3–C15 1.162(4).

than that in **4**, likely due to the conformation change of N<sub>2</sub>S<sub>2</sub> between **4** in which the two S atoms interact in the equatorial plane, while in **7** one S atom occupies an axial position with an elongated bonding interaction. In addition, the Pd–C<sub>ave</sub> bond distance (2.035 Å) is slightly longer than that in **4** as a result of the bridging ligation of tBuNC. Because the dinuclear Pd(I) complex **7** was formed upon the reduction of the mononuclear Pd(II) complex **4**, we wanted to probe whether the formation of **7** involves the transient formation of the **4-Pd<sup>I</sup>** species at room temperature; however the analysis of the electrolysis solution by EPR at different time points did not reveal the presence of paramagnetic species, suggesting that on the time scale of the electroreduction process at room temperature any **4-Pd<sup>I</sup>** species formed will dimerize rapidly to form **7**. This can also explain the low 12% yield obtained by spin integration of the EPR signal for the *in situ* formed **4-Pd<sup>I</sup>** species at  $-78\text{ }^\circ\text{C}$  (Table 1).

**Characterization of  $(^{\text{tBu}}\text{N}_4)\text{Pd}^{\text{I}}$  Species.** Because the  $(^{\text{tBu}}\text{N}_4)$  ligand was shown to stabilize paramagnetic Pd(III) complexes,<sup>32</sup> we also wanted to probe the possibility of employing such a ligand system for stabilizing Pd(I) species as a means to support a potential Pd(I)/Pd(III) catalytic cycle for chemical transformations. The  $[(^{\text{tBu}}\text{N}_4)\text{Pd}^{\text{II}}(\text{tBuNC})_2](\text{OTf})_2$  complex (**9**) was obtained as pink crystals by reacting  $[(^{\text{tBu}}\text{N}_4)\text{Pd}^{\text{II}}(\text{MeCN})_2](\text{OTf})_2$  (**8**)<sup>52</sup> with 2 equiv of tBuNC in MeCN (Scheme 2). The X-ray crystal structure reveals that the Pd(II) center has a distorted octahedral coordination geometry, similar to the structure of **8**:<sup>52</sup> the  $(^{\text{tBu}}\text{N}_4)$  ligand adopts a  $\kappa^4$  conformation with an axial elongation for the two amine N donor atoms, while the two tBuNC ligands are cis-positioned in the equatorial plane along with the two pyridine N donor atoms (Figure 6). The average Pd–N<sub>py</sub> bond length (2.061 Å) and the average Pd···N<sub>tBu</sub> distance (2.612 Å) are consistent with the previously reported values for **8**,<sup>52</sup> while the average Pd–CNtBu distance (1.950 Å) is slightly shorter than the average Pd–NCMe distance in **8**, likely due to the stronger donating ability of tBuNC vs MeCN.

Upon the chemical reduction of **8** and **9** by 1 equiv of  $\text{CoCp}_2$  at  $-35\text{ }^\circ\text{C}$  in MeCN:PrCN (1:3, v:v), the  $[(^{\text{tBu}}\text{N}_4)\text{Pd}^{\text{I}}\text{X}_2]^+$  species (X = MeCN, **8-Pd<sup>I</sup>**; X = tBuNC, **9-Pd<sup>I</sup>**) were observed by EPR, although the EPR signal for **8-Pd<sup>I</sup>** was quite faint (Figure 7 and Table 1). The axial pattern of the EPR spectra suggests that both Pd(I) centers exhibit a  $(d_{x^2-y^2})^1$

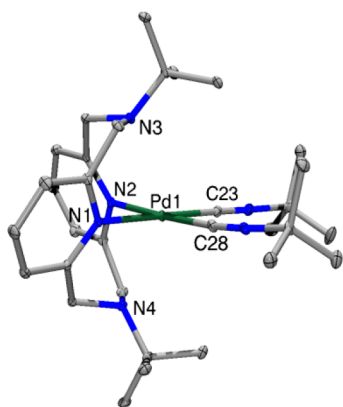


**Figure 6.** ORTEP representation of the cation of **9**, shown with 50% thermal ellipsoids and the triflate counteranions and H atoms omitted for clarity. Selected bond distances (Å) for **9**: Pd1–N1 2.063(2), Pd1–N2 2.059(2), Pd1–C23 1.946(3), Pd1–C28 1.954(3), Pd1...N3 2.610, Pd1...N4 2.614.

ground state, and the absence of N superhyperfine coupling from the  $^{t\text{Bu}}\text{N}$  groups to the Pd(I) center implies that upon the one-electron reduction the interaction with the axial N atoms is no longer present; that is, the conformation of the  $^{t\text{Bu}}\text{N4}$  ligand might change from  $\kappa^4$  to  $\kappa^2$ . To further probe this conformational change, we have performed DFT calculations for the **4-Pd<sup>I</sup>**,  $\kappa^4$ -**9-Pd<sup>I</sup>**, and  $\kappa^2$ -**9-Pd<sup>I</sup>** species and analyzed the interactions between the axial N atoms and the Pd(I) centers (Table 2).<sup>45</sup> When comparing the atomic orbital contributions to the frontier molecular orbitals of these complexes, we obtained for **4-Pd<sup>I</sup>** a 5% contribution from the axial pyridine N atom to the  $\beta$  lowest unoccupied molecular orbital (LUMO), supporting the observed superhyperfine coupling to the axial N in the EPR spectrum of **4-Pd<sup>I</sup>**. By comparison, for both  $\kappa^4$ -**9-Pd<sup>I</sup>** and  $\kappa^2$ -**9-Pd<sup>I</sup>** species in which the  $^{t\text{Bu}}\text{N4}$  ligand adopts  $\kappa^4$  and  $\kappa^2$  conformations, respectively, no contribution to the  $\beta$  LUMO from the axial N atomic orbitals was observed (Table 2), supporting the absence of any appreciable superhyperfine coupling to the axial N atoms. In addition, the EPR signal intensity for **9-Pd<sup>I</sup>** (98% yield by spin integration) is significantly stronger than **8-Pd<sup>I</sup>** (5% yield, Table 1 and Figure 7), suggesting that the presence of tBuNC stabilizes to a greater extent the Pd(I) center.

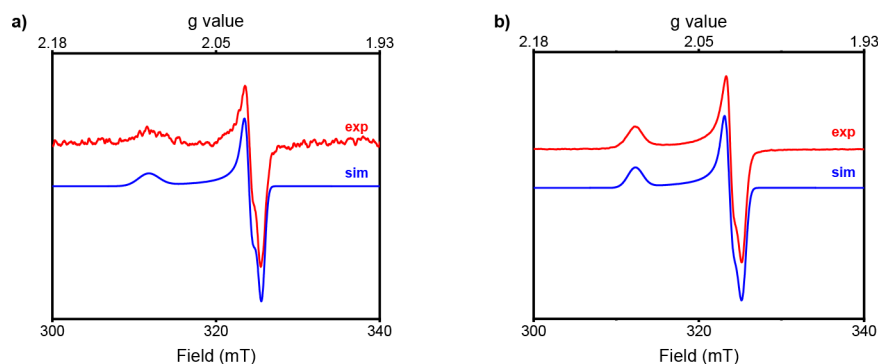
Palladium K-edge X-ray absorption spectroscopy (XAS), which involves excitation of Pd 1s electrons, has been shown to be an effective qualitative means of probing the formal

oxidation state for a systematic series of Pd complexes.<sup>53,54</sup>

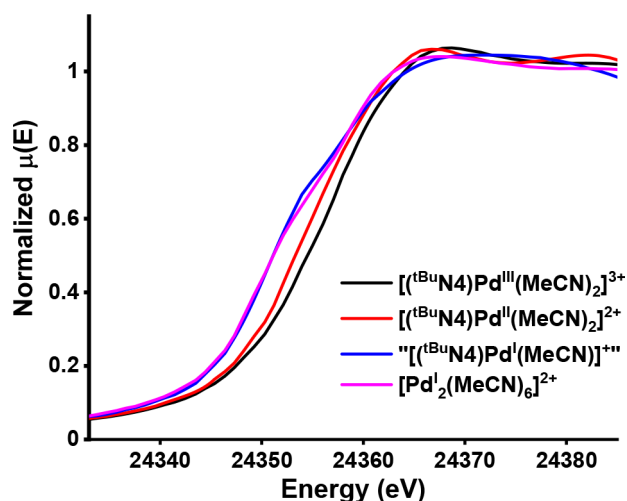
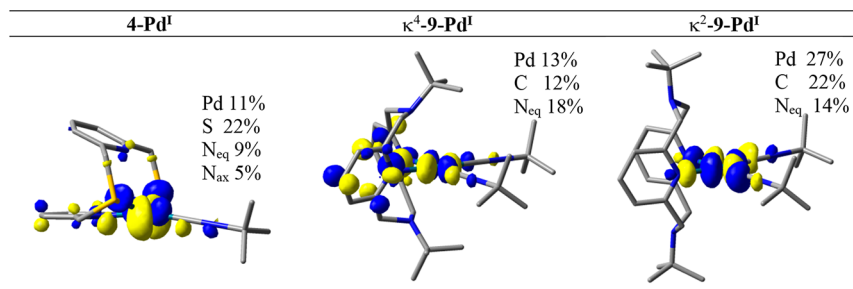
Because the EPR spectrum of **8-Pd<sup>I</sup>** reveals a weak signal (corresponding to a 5% yield based on spin integration, Table 1), to further probe the presence of a Pd(I) center, we have obtained XAS spectra for MeCN solutions of **8-Pd<sup>I</sup>** generated upon one-electron reduction at low temperature, the Pd(I) reference compound  $[\text{Pd}^{\text{I}}_2(\text{MeCN})_6]^{2+}$ ,<sup>55</sup> and the Pd(II) precursor  $[(^{t\text{Bu}}\text{N4})\text{Pd}^{\text{II}}(\text{MeCN})_2]^{2+}$  (**8**) and the Pd(III) species  $[(^{t\text{Bu}}\text{N4})\text{Pd}^{\text{III}}(\text{MeCN})_2]^{3+}$  formed upon electrochemical oxidation of **8** (Figure 8).<sup>52</sup> Interestingly, an increase in the edge energy is observed with increasing oxidation state of the Pd center (24352, 24354, and 24355.5 eV for Pd(I), Pd(II), and Pd(III), respectively), confirming that in this case the XAS edge energy correlates with the formal oxidation state assignment. Moreover, the edge energy of **8-Pd<sup>I</sup>** matches very closely the edge energy observed for  $[\text{Pd}^{\text{I}}_2(\text{MeCN})_6]^{2+}$ , supporting the formation of either mononuclear or dinuclear Pd(I) species upon the reduction of **8**. The presence of a weak EPR signal for **8-Pd<sup>I</sup>** could be also due to the formation of a dinuclear Pd(I) species either containing a Pd–Pd bond—commonly observed for Pd(I) complexes—or in which the two Pd(I) centers are antiferromagnetically coupled through bridging ligand(s), similar to **7** (*vide supra*). It is important to note that these XAS studies were employed mainly to probe the overall formal oxidation state of the resulting Pd species upon the one-electron reduction of **8**, and the results strongly suggest the formation of Pd(I) species, without subsequent disproportionation or oxidation of these Pd(I) species. While these studies do not provide structural information for the various Pd(I) species formed *in situ*, they lead us to suggest that one approach to further stabilize mononuclear Pd(I) species and to disfavor dimerization could be the use of bulkier, sterically hindered ancillary or exogenous ligands.

## CONCLUSION

In summary, reported herein is a thorough spectroscopic characterization of a series of  $(\text{N}2\text{S}2)\text{Pd}^{\text{I}}$  and  $(^{t\text{Bu}}\text{N}4)\text{Pd}^{\text{I}}$  complexes. We have shown that the Pd(I) oxidation state is accessible for all the studied Pd(II) complexes via either chemical or electrochemical reduction. EPR, UV–vis, and X-ray absorption spectroscopy provide direct evidence for the presence of Pd(I) intermediates, for which the stability was further improved with the assistance of a series of soft isonitrile and phosphine ligands. The proposed structures based on the simulations of the EPR data were further corroborated by DFT calculations. Moreover, an uncommon diamagnetic Pd(I)–



**Figure 7.** Experimental and simulated EPR spectra of reaction mixtures of  $(^{t\text{Bu}}\text{N}4)\text{Pd}^{\text{II}}$  complexes **8** and **9** with 1 equiv of  $\text{CoCp}_2$  at 77 K in 1:3 MeCN:PrCN frozen glass: (a) **8** +  $\text{CoCp}_2$ ; (b) **9** +  $\text{CoCp}_2$ . The parameters used for the simulations can be found in Table 1.

Table 2. Comparison of the  $\beta$  Lowest Unoccupied Molecular Orbitals (LUMOs) of  $4\text{-Pd}^{\text{I}}$ ,  $\kappa^4\text{-9-Pd}^{\text{I}}$ , and  $\kappa^2\text{-9-Pd}^{\text{I}}$  Complexes

**Figure 8.** Edge region of the X-ray absorption spectra for  $8\text{-Pd}^{\text{I}}$  (or a dinuclear  $\text{Pd}^{\text{I}}$  species generically labeled  $[(\text{tBuN}4)\text{Pd}^{\text{II}}(\text{MeCN})]^{+}$ ), the  $\text{Pd}^{\text{I}}$  reference compound  $[\text{Pd}^{\text{I}}_2(\text{MeCN})_6]^{2+}$ ,  $[(\text{tBuN}4)\text{Pd}^{\text{II}}(\text{MeCN})_2]^{2+}$  (**8**), and the  $\text{Pd}^{\text{III}}$  species  $[(\text{tBuN}4)\text{Pd}^{\text{III}}(\text{MeCN})_2]^{3+}$ .

$\text{Pd}^{\text{I}}$  dinuclear species with two bridging  $\text{tBuNC}$  ligands was isolated via electrochemical reduction of **4** and structurally characterized. Taking advantage of these results, we are currently further optimizing the reactions conditions and the ligands employed for isolating a range of mononuclear  $\text{Pd}^{\text{I}}$  complexes, with the goal of investigating in detail their stoichiometric reactivity and catalytic applications.

## EXPERIMENTAL DETAILS

**Ligand and Metal Complex Syntheses. Reagents and Materials.** All chemicals were commercially available from Aldrich, Fisher, or Strem Chemicals and were used as received without further purification. 2,11-Dithia[3.3](2,6)pyridinophane ( $\text{N}2\text{S}2$ ),<sup>37,41,56</sup>  $N,N'$ -ditertbutyl-2,11-diaza[3.3](2,6)pyridinophane ( $\text{tBuN}4$ ),<sup>57</sup>  $[(\text{N}2\text{S}2)\text{Pd}^{\text{II}}(\text{MeCN})_2](\text{OTf})_2$  (**1**),<sup>39</sup>  $[(\text{N}2\text{S}2)\text{Pd}^{\text{II}}\text{Me}]_2(\text{OTf})_2$  (**2**),<sup>39</sup>  $[(\text{N}2\text{S}2)\text{Pd}^{\text{II}}\text{Cl}](\text{OTf})$  (**3**),<sup>37</sup> and  $[(\text{tBuN}4)\text{Pd}^{\text{II}}(\text{MeCN})_2](\text{OTf})_2$  (**8**)<sup>52</sup> were prepared according to the literature procedures. Solvents were purified prior to use by passing through a column of activated alumina using an MBraun solvent purification system. On the basis of their reduction potential,<sup>58</sup> either cobaltocene ( $\text{CoCp}_2$ ) or bis(pentamethyl)cyclopentadienyl cobalt(II) ( $\text{CoCp}^*_2$ ) was used as a reducing agent.

$[(\text{N}2\text{S}2)\text{Pd}^{\text{II}}(\text{tBuNC})](\text{OTf})_2$ , **4**. 2 equiv of  $\text{tBuNC}$  (8.1  $\mu\text{L}$ , 70.2  $\mu\text{mol}$ ) was added via a microsyringe to a  $\text{MeCN}$  solution (2 mL) of  $[(\text{N}2\text{S}2)\text{Pd}^{\text{II}}(\text{MeCN})_2](\text{OTf})_4$  (50.4 mg, 35.0  $\mu\text{mol}$ ) while stirring. The solution changed color from brown to red immediately. After 1 h, the solvent was removed under vacuum, and the resulting red oil was stored at  $-20^\circ\text{C}$  for 1 h to give a needle-shaped red crystalline product. Yield: 52.8 mg, 89%.  $^1\text{H NMR}$  ( $\text{CD}_3\text{CN}$ , 300 MHz),  $\delta$

(ppm): 1.66 (s, 9H,  $\text{tBu}$ ), 4.62 (d,  $J = 16.5$  Hz, 4H,  $\text{CH}_2$ ), 5.08 (d,  $J = 16.5$  Hz, 4H,  $\text{CH}_2$ ), 7.24 (d,  $J = 7.8$  Hz, 4H,  $\text{Py H}_{\text{meta}}$ ), 7.62 (t,  $J = 8.1$  Hz, 2H,  $\text{Py H}_{\text{para}}$ ). UV-vis ( $\text{MeCN}$ ;  $\lambda$ , nm ( $\epsilon$ ,  $\text{M}^{-1}\text{cm}^{-1}$ ): 327 (3200), 497 (200). Elemental analysis: found, C 34.06, H 2.98, N 6.40%; calculated  $\text{C}_{21}\text{H}_{23}\text{F}_6\text{N}_3\text{O}_6\text{PdS}_4 \cdot 0.5\text{CH}_3\text{CN}$ , C 33.76, H 3.16, N 6.26%. ESI-MS ( $m/z$ ): 462.0314, calculated for  $[(\text{N}2\text{S}2)\text{Pd}^{\text{II}}(\text{tBuNC})\text{H}^+]^+$ : 462.0290.

$[(\text{N}2\text{S}2)\text{Pd}^{\text{II}}(\text{PPh}_3)](\text{OTf})_2$ , **5**. 2 equiv  $\text{PPh}_3$  (10.2 mg, 39.0  $\mu\text{mol}$ ) was dissolved in 2 mL of  $\text{MeCN}$  and added to a  $\text{MeCN}$  solution (2 mL) of  $[(\text{N}2\text{S}2)\text{Pd}^{\text{II}}(\text{MeCN})_2](\text{OTf})_4$  (28.1 mg, 19.5  $\mu\text{mol}$ ) while stirring. The solution changed color from brown to red immediately. After 1 h, the mixture was set up for crystallization with anhydrous diethyl ether vapor diffusion at room temperature. A needle-shaped red crystalline product formed after 1–2 days. Yield: 29.9 mg, 82%.  $^1\text{H NMR}$  ( $\text{CD}_3\text{CN}$ , 300 MHz),  $\delta$  (ppm): 4.42 (d,  $J = 16.5$  Hz, 4H,  $\text{CH}_2$ ), 4.58 (d,  $J = 16.2$  Hz, 4H,  $\text{CH}_2$ ), 7.18 (d,  $J = 7.8$  Hz, 4H,  $\text{Py H}_{\text{meta}}$ ), 7.59 (t,  $J = 7.8$  Hz, 2H,  $\text{Py H}_{\text{para}}$ ), 7.6–7.9 (m, 15H, Ph). UV-vis ( $\text{MeCN}$ ;  $\lambda$ , nm ( $\epsilon$ ,  $\text{M}^{-1}\text{cm}^{-1}$ ): 317 (sh, 6600), 392 (sh, 1360), 503 (630). Elemental analysis: found, C 43.66, H 2.96, N 4.00%; calculated  $\text{C}_{34}\text{H}_{29}\text{F}_6\text{N}_3\text{O}_6\text{PPdS}_4 \cdot 0.5\text{CH}_3\text{CN}$ , C 43.71, H 3.20, N 3.64%. ESI-MS ( $m/z$ ): 321.0275, calculated for  $[(\text{N}2\text{S}2)\text{Pd}^{\text{II}}(\text{PPh}_3)]^{2+}$ : 321.0273.

$[(\text{N}2\text{S}2)\text{Pd}^{\text{II}}\text{Me}(\text{PPh}_3)](\text{OTf})_2$ , **6**. A 0.5 mL  $\text{MeCN}$  solution of 2 equiv of  $\text{PPh}_3$  (8.2 mg, 31.2  $\mu\text{mol}$ ) was added dropwise to a  $\text{MeCN}$  solution (2 mL) of  $[(\text{N}2\text{S}2)\text{Pd}^{\text{II}}\text{Me}]_2(\text{OTf})_2$  (17.0 mg, 15.6  $\mu\text{mol}$ ) while stirring. The solution changed color from orange to light yellow immediately. After 0.5 h, the mixture was set up for crystallization with diethyl ether vapor diffusion at room temperature (RT). Square-shaped colorless crystalline formed after 1–2 days. Yield: 15.0 mg, 60%.  $^1\text{H NMR}$  ( $\text{CD}_3\text{CN}$ , 300 MHz),  $\delta$  (ppm): 0.75 (d,  $J_{\text{P-H}} = 3$  Hz, 3H, Me), 3.94 (br, 2H,  $\text{CH}_2$ ), 4.48 (br, 2H,  $\text{CH}_2$ ), 4.92 (br, 2H,  $\text{CH}_2$ ), 5.30 (br, 2H,  $\text{CH}_2$ ), 7.00 (br, 2H,  $\text{Py H}_{\text{meta}}$ ), 7.4–7.6 (m, 15H, Ph), 7.77 (br, 1H,  $\text{Py H}_{\text{para}}$ ). Another set of  $\text{Py H}_{\text{meta}}$  and  $\text{H}_{\text{para}}$  peaks are buried under the peak corresponding to the Ph groups. UV-vis ( $\text{MeCN}$ ;  $\lambda$ , nm ( $\epsilon$ ,  $\text{M}^{-1}\text{cm}^{-1}$ ): 292 (1300),  $\sim 320$  (sh, 430),  $\sim 406$  (sh, 20). Elemental analysis: found, C 50.67, H 3.61, N 3.42%; calculated  $\text{C}_{34}\text{H}_{32}\text{F}_3\text{N}_3\text{O}_3\text{PPdS}_3$ , C 50.59, H 4.00, N 3.47%. ESI-MS ( $m/z$ ): 657.0784, calculated for  $[(\text{N}2\text{S}2)\text{Pd}^{\text{II}}\text{Me}(\text{PPh}_3)]^+$ : 657.0779.

$[(\text{N}2\text{S}2)\text{Pd}^{\text{II}}(\mu\text{-tBuNC})_2](\text{ClO}_4)_2$ , **7**. Electrochemical reduction of  $[(\text{N}2\text{S}2)\text{Pd}^{\text{II}}(\text{tBuNC})](\text{OTf})_2$  (27.7 mg, 36.3  $\mu\text{mol}$ ) was performed in 10 mL of 0.1 M  $(\text{Bu}_4\text{N})\text{ClO}_4$  in  $\text{MeCN}$  at RT under  $\text{N}_2$ . The color changed from red to yellowish orange during the electrolysis. After the charge corresponding to  $1e^-$  reduction has passed, the electrolysis was stopped and the solution was concentrated to  $\sim 1$  mL under vacuum. The resulting orange solution was stored at  $-35^\circ\text{C}$  for several days. Orange needle-shaped crystals were collected by filtration and washed with pentane. Yield: 6.3 mg, 30%.  $^1\text{H NMR}$  ( $\text{CD}_3\text{CN}$ , 300 MHz),  $\delta$  (ppm): 0.75 (s, 18H,  $\text{tBu}$ ), 4.55 (d,  $J = 15.9$  Hz, 8H,  $\text{CH}_2$ ), 4.95 (br,  $J = 15.9$  Hz, 8H,  $\text{CH}_2$ ), 7.30 (d,  $J = 6.9$  Hz, 8H,  $\text{Py H}_{\text{meta}}$ ), 7.70 (t, br,  $J = 7.2$  Hz, 4H,  $\text{Py H}_{\text{para}}$ ). UV-vis ( $\text{MeCN}$ ;  $\lambda$ , nm ( $\epsilon$ ,  $\text{M}^{-1}\text{cm}^{-1}$ ): 365 (3400). Elemental analysis: found, C 42.12, H 4.13, N 8.90%; calculated  $\text{C}_{40}\text{H}_{48}\text{Cl}_2\text{N}_6\text{O}_8\text{Pd}_2\text{S}_4 \cdot 1.5\text{CH}_3\text{CN}$ , C 42.53, H 4.36, N 8.65%. ESI-MS ( $m/z$ ): 463.0359, calculated for  $[(\text{N}2\text{S}2)\text{Pd}^{\text{I}}(\text{tBuNC})]^+$ : 463.0368.

$[(tBu_4N)Pd^{II}(tBuNC)_2](OTf)_2$ , **9**. 2 equiv of  $tBuNC$  (5.4  $\mu L$ , 47.7  $\mu mol$ ) was added through a microsyringe to an MeCN solution (1 mL) of  $[(tBu_4N)Pd^{II}(MeCN)_2](OTf)_2$  (20.1 mg, 24.0  $\mu mol$ ) while stirring. The solution changed color from blue to pink immediately. After 30 min, the solvent was removed, and the resulting pink crystalline solid was dried under vacuum. Yield: 22.0 mg, 100%.  $^1H$  NMR ( $CD_3CN$ , 300 MHz),  $\delta$  (ppm): 1.46 (s, 18H,  $tBu-NC$ ), 1.47 (s, 18H,  $tBu-N4$ ), 3.57 (d,  $J = 17.1$  Hz, 4H,  $CH_2$ ), 4.64 (d,  $J = 17.4$  Hz, 4H,  $CH_2$ ), 7.31 (d,  $J = 8.1$  Hz, 4H,  $Py H_{meta}$ ), 7.85 (t,  $J = 8.1$  Hz, 2H,  $Py H_{para}$ ). UV–vis (MeCN;  $\lambda$ , nm ( $\epsilon$ ,  $M^{-1} cm^{-1}$ ): 489 (70), 343 (sh, 250). Elemental analysis: found, C 44.08, H 4.93, N 8.98%; calculated  $C_{34}H_{50}F_6N_6O_6PdS_2$ , C 44.23, H 5.46, N 9.10%. ESI-MS ( $m/z$ ): 229.0833, calculated for  $[(tBu_4N)Pd^{II}]^{2+}$ : 229.0831; 270.6199, calculated for  $[(tBu_4N)Pd^{II}(tBuNC)]^{2+}$ : 270.6199; 312.1567, calculated for  $[(tBu_4N)Pd^{II}(tBuNC)_2]^{2+}$ : 312.1566; 773.2652, calculated for  $[(tBu_4N)Pd^{II}(tBuNC)_2](OTf)^+$ : 773.2652.

**Physical Measurements. General Methods.**  $^1H$  (300.121 MHz) NMR spectra were recorded on a Varian Mercury-300 spectrometer. Low-temperature ( $-20$  °C)  $^1H$  (600 MHz) NMR spectra were recorded on a Varian Unity Inova-600 spectrometer. Chemical shifts are reported in ppm and referenced to residual solvent resonance peaks. Abbreviations for the multiplicity of NMR signals are s (singlet), d (doublet), t (triplet), q (quartet), sep (septet), m (multiplet), and br (broad). UV–vis spectra were recorded on a Varian Cary 50 Bio spectrophotometer. EPR spectra were recorded on a JEOL JES-FA X-band (9.2 GHz) EPR spectrometer in MeCN:PrCN (v:v = 1: 3) frozen glass at 77 K. Simulation of EPR spectra was performed by using WinEPR SimFonia v.1.25. Elemental analyses were performed by the Columbia Analytical Services Tucson Laboratory. ESI-MS experiments were performed on a Bruker Maxis QTOF mass spectrometer with an electron spray ionization source. ESI mass spectrometry was provided by Washington University Mass Spectrometry Resource, a NIH Research Resource (Grant P41RR0954).

**Electrochemical Measurements.** Electrochemical grade ( $Bu_4N$ )- $ClO_4$  purchased from Aldrich was used as the supporting electrolyte. Cyclic voltammetry was performed with a BASi EC Epsilon electrochemical workstation or a CHI 660D electrochemical analyzer. Electrochemical measurements were performed under a flow of nitrogen, and the analyzed solutions were deaerated by purging with nitrogen. A glassy carbon electrode (GCE,  $d = 1.6$  mm) was used as the working electrode, while a Pt wire was used as the auxiliary electrode. The nonaqueous reference electrode containing Ag/0.01 M  $AgNO_3$  in 0.1 M  $Bu_4NClO_4$ /MeCN was calibrated against Fc; the potential of the  $Fc^+/Fc$  couple vs Ag/0.01 M  $AgNO_3$ /0.1 M  $Bu_4NClO_4$ /MeCN reference electrode is +0.105 V.

**EPR Studies of the In Situ Formation of the Pd(I) Species.** An EPR tube was charged with a solution of Pd complex in MeCN:PrCN (v:v = 1: 3) and cooled to  $-78$  °C in a dry ice/acetone bath. Another solution containing 1 equiv of chemical reducing agent ( $CoCp_2$  or  $CoCp^*_2$ ) in the same solvent mixture was quickly added via a microsyringe, followed by a quick shake of the tube, and then the sample was frozen in the liquid nitrogen. An initial EPR spectrum was taken at 77 K. The sample was then carefully warmed for 10–30 s to allow for the complete reaction to occur and refrozen; the EPR spectrum was recorded again, or the sample was warmed for longer times to probe the thermal stability of the generated Pd(I) species (Figure S9).

**Computational Studies.** The density functional theory (DFT) calculations were performed with the program package Gaussian 09.<sup>59</sup> The B3LYP functional was employed,<sup>60,61</sup> and the Stevens (CEP-31G)<sup>62,63</sup> valence basis set and effective core potential were used for Pd,<sup>64,65</sup> which have been shown previously to reproduce well experimental parameters of Pd complexes,<sup>66,67</sup> and have been used by us previously and shown to predict well the electronic properties of paramagnetic Pd complexes.<sup>32–38</sup> We have also employed the B3LYP-D3 and M06 functionals and other electron core potential basis sets; however, the calculated atomic contribution to the frontier MOs varied only slightly. The geometry optimization calculations used were performed for the cations of **4-Pd<sup>I</sup>**,  **$\kappa^4$ -9-Pd<sup>I</sup>**, and  **$\kappa^2$ -9-Pd<sup>I</sup>**, based

on the crystallographic coordinates of the cations of **4**, **9**, and a proposed conformation of  **$\kappa^2$ -9**, respectively. The ground state wave functions were investigated by analysis of the frontier MOs, and the atomic contributions to MOs were calculated by using the program Chemissian.<sup>68</sup>

**X-ray Absorption Spectroscopy (XAS) Studies.** The XAS measurements were conducted at Argonne National Laboratory (Argonne, IL), at the Advanced Photon Source (ring energy = 7.0 GeV) on the 10-ID beamline of the Materials Research Collaborative Access Team (MRCAT). The samples were loaded into a custom-designed, chemically resistant PEEK cell fitted with a cap with a Swagelok VCR fitting and a hand-tightened O-ring seal.<sup>53</sup> The temperature- and air-sensitive samples were loaded under a nitrogen blanket in a dry ice bath. The solution measurements were made in emission mode. The experiments utilized a cryogenically cooled double-crystal Si(111) monochromator in conjunction with a glass-coated mirror to minimize the presence of harmonics. The monochromator was scanned continuously from  $-200$  to  $+800$  eV relative to the Pd  $k$ -edge energy. Scans were taken with a Pd<sup>0</sup> foil reference (24352.6 eV) for energy correction during data analysis (see below).

**XAS Spectral Processing and Analysis.** The program Athena (Athena Ravel REF) was used to process the XANES spectra. The sample and Pd foil reference spectra were imported, and background removal and normalization was performed. Then, the Pd foil reference for every sample spectrum was energy corrected by selecting the maximum in the first derivative, finding the zero crossing in the second derivative, and setting the energy of the zero crossing to 24352.6 eV. The energy-corrected Pd foil reference spectra were then aligned to have all sample data on the same absolute energy grid for analysis purposes.

**X-ray Diffraction Studies.** Crystals of X-ray diffraction quality were obtained by slow anhydrous diethyl ether vapor diffusion into acetonitrile solutions. Suitable crystals of appropriate dimensions were mounted on Mitgen loops in random orientations. Preliminary examination and data collection were performed by using a Bruker Kappa Apex-II charge coupled device (CCD) detector system single crystal X-ray diffractometer equipped with an Oxford Cryostream LT device. Data were collected by using graphite monochromated Mo K radiation ( $= 0.71073$  Å) from a fine focus sealed tube X-ray source. Preliminary unit cell constants were determined with a set of 36 narrow frame scans. Typical data sets consist of a combination of  $\omega$  and  $\varphi$  scan frames with typical scan width of 0.5 and counting time of 15–30 s/frame at a crystal-to-detector distance of  $\sim 4.0$  cm. The collected frames were integrated by using an orientation matrix determined from the narrow frame scans. Apex II and SAINT software packages were used for data collection and data integration.<sup>70</sup> Analysis of the integrated data did not show any decay. Final cell constants were determined by global refinement of reflections from the complete data set. Data were corrected for systematic errors by using SADABS based on the Laue symmetry using equivalent reflections.<sup>70</sup>

## ■ ASSOCIATED CONTENT

### Supporting Information

The Supporting Information is available free of charge at <https://pubs.acs.org/doi/10.1021/acs.inorgchem.0c01938>.

Reactivity studies of reduction of **2** and **6** by  $^1H$  NMR, time-dependent EPR spectra of the mixture of **4** and  $CoCp_2$ , computational details, and X-ray crystal structure data (PDF)

### Accession Codes

CCDC 1569571–1569575 contain the supplementary crystallographic data for this paper. These data can be obtained free of charge via [www.ccdc.cam.ac.uk/data\\_request/cif](http://www.ccdc.cam.ac.uk/data_request/cif), or by emailing [data\\_request@ccdc.cam.ac.uk](mailto:data_request@ccdc.cam.ac.uk), or by contacting The Cambridge Crystallographic Data Centre, 12 Union Road, Cambridge CB2 1EZ, UK; fax: +44 1223 336033.

## AUTHOR INFORMATION

## Corresponding Author

Liviu M. Mirica – Department of Chemistry, University of Illinois at Urbana–Champaign, Urbana, Illinois 61801, United States; [orcid.org/0000-0003-0584-9508](https://orcid.org/0000-0003-0584-9508); Email: [mirica@illinois.edu](mailto:mirica@illinois.edu)

## Authors

Jia Luo – Department of Chemistry, Washington University, St. Louis, Missouri 63130-4899, United States

Giang N. Tran – Department of Chemistry, University of Illinois at Urbana–Champaign, Urbana, Illinois 61801, United States

Nigam P. Rath – Department of Chemistry and Biochemistry, University of Missouri, St. Louis, Missouri 63121-4400, United States

Complete contact information is available at:

<https://pubs.acs.org/10.1021/acs.inorgchem.0c01938>

## Notes

The authors declare no competing financial interest.

## ACKNOWLEDGMENTS

We thank the Department of Energy's BES Catalysis Science Program (DE-SC0006862) for financial support. We also thank Drs. Jeffrey T. Miller and Ryan C. Nelson (Argonne National Lab) for assistance with obtaining the XAS data and Dr. Jason Schultz for assistance with the EPR measurements.

## REFERENCES

- (1) Negishi, E. *Handbook of Organopalladium Chemistry for Organic Synthesis*; John Wiley & Sons: Hoboken, NJ, 2002; 3424 pp.
- (2) Hartwig, J. F. *Organotransition Metal Chemistry: From Bonding to Catalysis*; University Science Books: Sausalito, CA, 2010; 1127 pp.
- (3) Lyons, T. W.; Sanford, M. S. Palladium-Catalyzed Ligand-Directed C-H Functionalization Reactions. *Chem. Rev.* **2010**, *110*, 1147–1169.
- (4) Muñiz, K. High-Oxidation-State Palladium Catalysis: New Reactivity for Organic Synthesis. *Angew. Chem., Int. Ed.* **2009**, *48*, 9412–9423.
- (5) Cauty, A. J. Organopalladium and platinum chemistry in oxidising milieu as models for organic synthesis involving the higher oxidation states of palladium. *J. Chem. Soc., Dalton Trans.* **2009**, 10409–17.
- (6) Chen, X.; Engle, K. M.; Wang, D. H.; Yu, J. Q. Palladium(II)-Catalyzed C-H Activation/C-C Cross-Coupling Reactions: Versatility and Practicality. *Angew. Chem., Int. Ed.* **2009**, *48*, 5094–5115.
- (7) Sehna, P.; Taylor, R. J. K.; Fairlamb, I. J. S. Emergence of Palladium(IV) Chemistry in Synthesis and Catalysis. *Chem. Rev.* **2010**, *110*, 824–889.
- (8) Desai, L. V.; Hull, K. L.; Sanford, M. S. Palladium-catalyzed oxygenation of unactivated sp(3) C-H bonds. *J. Am. Chem. Soc.* **2004**, *126*, 9542–9543.
- (9) Xu, L.-M.; Li, B.-J.; Yang, Z.; Shi, Z.-J. Organopalladium(IV) chemistry. *Chem. Soc. Rev.* **2010**, *39*, 712–733.
- (10) Powers, D. C.; Ritter, T. Palladium(III) in Synthesis and Catalysis. *Top. Organomet. Chem.* **2011**, *35*, 129–156.
- (11) Mirica, L. M.; Khusnutdinova, J. R. Structure and electronic properties of Pd(III) complexes. *Coord. Chem. Rev.* **2013**, *257*, 299–314.
- (12) Shaughnessy, K. H. Development of Palladium Precatalysts that Efficiently Generate LPd(0) Active Species. *Isr. J. Chem.* **2020**, *60*, 180–194.
- (13) Bonney, K. J.; Proutiere, F.; Schoenebeck, F. Dinuclear Pd(I) complexes-solely precatalysts? Demonstration of direct reactivity of a Pd(I) dimer with an aryl iodide. *Chem. Sci.* **2013**, *4*, 4434–4439.
- (14) Chen, X. Y.; Pu, M. P.; Cheng, H. G.; Sperger, T.; Schoenebeck, F. Arylation of Axially Chiral Phosphorothioate Salts by Dinuclear Pd-I Catalysis. *Angew. Chem., Int. Ed.* **2019**, *58*, 11395–11399.
- (15) Liu, Q.; Dong, X.; Li, J.; Xiao, J.; Dong, Y. H.; Liu, H. Recent Advances on Palladium Radical Involved Reactions. *ACS Catal.* **2015**, *5*, 6111–6137.
- (16) Vilar, R.; Mingos, D. M. P.; Cardin, C. J. Synthesis and structural characterization of [Pd<sub>2</sub>(P-Br)<sub>2</sub>(PBut<sub>3</sub>)<sub>2</sub>], an example of a palladium(I)-palladium(I) dimer. *J. Chem. Soc., Dalton Trans.* **1996**, 4313–4314.
- (17) Hruszkewycz, D. P.; Wu, J.; Hazari, N.; Incarvito, C. D. Palladium(I)-bridging allyl dimers for the catalytic functionalization of CO<sub>2</sub>. *J. Am. Chem. Soc.* **2011**, *133*, 3280–3283.
- (18) Aufiero, M.; Proutiere, F.; Schoenebeck, F. Redox Reactions in Palladium Catalysis: On the Accelerating and/or Inhibiting Effects of Copper and Silver Salt Additives in Cross-Coupling Chemistry Involving Electron-rich Phosphine Ligands. *Angew. Chem., Int. Ed.* **2012**, *51*, 7226–7230.
- (19) Proutiere, F.; Aufiero, M.; Schoenebeck, F. Reactivity and Stability of Dinuclear Pd(I) Complexes: Studies on the Active Catalytic Species, Insights into Precatalyst Activation and Deactivation, and Application in Highly Selective Cross-Coupling Reactions. *J. Am. Chem. Soc.* **2012**, *134*, 606–612.
- (20) Kalvet, I.; Bonney, K. J.; Schoenebeck, F. Kinetic and Computational Studies on Pd(I) Dimer-Mediated Halogen Exchange of Aryl Iodides. *J. Org. Chem.* **2014**, *79*, 12041–12046.
- (21) Yin, G. Y.; Kalvet, I.; Schoenebeck, F. Trifluoromethylthiolation of Aryl Iodides and Bromides Enabled by a Bench-Stable and Easy-To-Recover Dinuclear Palladium(I) Catalyst. *Angew. Chem., Int. Ed.* **2015**, *54*, 6809–6813.
- (22) Simpson, Q.; Sinclair, M. J. G.; Lupton, D. W.; Chaplin, A. B.; Hooper, J. F. Oxidative Cross-Coupling of Boron and Antimony Nucleophiles via Palladium(I). *Org. Lett.* **2018**, *20*, 5537–5540.
- (23) Fujiwara, S.; Nakamura, M. Electron Spin Resonance of Pd(I). 2. Gamma-Irradiated Single Crystals of K<sub>2</sub>pdCl<sub>4</sub> and (NH<sub>4</sub>)<sub>2</sub>pdCl<sub>4</sub>. *J. Chem. Phys.* **1971**, *54*, 3378–3380.
- (24) Broadley, K.; Lane, G. A.; Connelly, N. G.; Geiger, W. E. Electrochemical routes to paramagnetic dinuclear and mononuclear palladium  $\dot{\text{I}}\text{c}$  complexes stabilized by the pentaphenylcyclopentadienyl ligand. *J. Am. Chem. Soc.* **1983**, *105*, 2486–7.
- (25) Lane, G. A.; Geiger, W. E.; Connelly, N. G. Palladium(I). pi-radicals. Electrochemical preparation and study of their reaction pathways. *J. Am. Chem. Soc.* **1987**, *109*, 402–407.
- (26) Blake, A. J.; Gould, R. O.; Hyde, T. I.; Schröder, M. Stabilization of monovalent palladium by tetraaza macrocycles. *J. Chem. Soc., Chem. Commun.* **1987**, *0*, 431–3.
- (27) Blake, A. J.; Gould, R. O.; Hyde, T. I.; Schröder, M. Tetrahedral Distortion in Palladium(II) Macrocyclic Complexes: The Single Crystal X-Ray Structure of [Pd(tbc)](PF<sub>6</sub>)<sub>2</sub> = 0.4MeNO<sub>2</sub> (tbc = 1,4,8,11-tetrabenzyl-1,4,8,11-tetra-azacyclotetradecane). *J. Chem. Soc., Chem. Commun.* **1987**, 1730–1732.
- (28) Reid, G.; Blake, A. J.; Hyde, T. I.; Schröder, M. Stereochemical and redox properties of palladium complexes of 1,4,10,13-tetrathia-7,16-diazacyclooctadecane. *J. Chem. Soc., Chem. Commun.* **1988**, 1397–9.
- (29) MacInnis, M. C.; DeMott, J. C.; Zolnhofer, E. M.; Zhou, J.; Meyer, K.; Hughes, R. P.; Ozerov, O. V. Cationic Two-Coordinate Complexes of Pd(I) and Pt(I) Have Longer Metal-Ligand Bonds Than Their Neutral Counterparts. *Chem.* **2016**, *1*, 902–920.
- (30) Troadec, T.; Tan, S. Y.; Wedge, C. J.; Rourke, J. P.; Unwin, P. R.; Chaplin, A. B. One-Electron Oxidation of [M((PBu<sub>3</sub>)-Bu-t)(2)] (M = Pd, Pt): Isolation of Monomeric [Pd((PBu<sub>3</sub>)-Bu-t)(2)](+) and Redox-Promoted C-H Bond Cyclometalation. *Angew. Chem., Int. Ed.* **2016**, *55*, 3754–3757.
- (31) Fenske, D.; Bensmann, W. Preparation and Crystal Structure of Mononuclear, Paramagnetic Pd and Pt Complexes. *Z. Naturforsch., B: J. Chem. Sci.* **1985**, *40*, 1093–1096.

- (32) Khusnutdinova, J. R.; Rath, N. P.; Mirica, L. M. Stable Mononuclear Organometallic Pd(III) Complexes and Their C-C Bond Formation Reactivity. *J. Am. Chem. Soc.* **2010**, *132*, 7303–7305.
- (33) Khusnutdinova, J. R.; Rath, N. P.; Mirica, L. M. Dinuclear Palladium(III) Complexes with a Single Unsupported Bridging Halide Ligand: Reversible Formation from Mononuclear Palladium(II) or Palladium(IV) Precursors. *Angew. Chem., Int. Ed.* **2011**, *50*, 5532–5536.
- (34) Khusnutdinova, J. R.; Rath, N. P.; Mirica, L. M. The Aerobic Oxidation of a Pd(II) Dimethyl Complex Leads to Selective Ethane Elimination from a Pd(III) Intermediate. *J. Am. Chem. Soc.* **2012**, *134*, 2414–2422.
- (35) Tang, F.; Qu, F.; Khusnutdinova, J. R.; Rath, N. P.; Mirica, L. M. Structural and Reactivity Comparison of Analogous Organometallic Pd(III) and Pd(IV) Complexes. *Dalton Trans.* **2012**, *41*, 14046–14050.
- (36) Khusnutdinova, J. R.; Qu, F.; Zhang, Y.; Rath, N. P.; Mirica, L. M. Formation of the Pd(IV) Complex [(Me3tacn)PdIVMe3]+ through Aerobic Oxidation of (Me3tacn)PdII Me2 (Me3tacn = N, N', N''-trimethyl-1,4,7-triazacyclononane). *Organometallics* **2012**, *31*, 4627–4630.
- (37) Luo, J.; Rath, N. P.; Mirica, L. M. Oxidative Reactivity of (N2S2)PdRX Complexes (R = Me, Cl; X = Me, Cl, Br): Involvement of Palladium(III) and Palladium(IV) Intermediates. *Organometallics* **2013**, *32*, 3343–3353.
- (38) Tang, F.; Zhang, Y.; Rath, N. P.; Mirica, L. M. Detection of Pd(III) and Pd(IV) Intermediates during the Aerobic Oxidative C-C Bond Formation from a Pd(II) Dimethyl Complex. *Organometallics* **2012**, *31*, 6690–6696.
- (39) Luo, J.; Khusnutdinova, J. R.; Rath, N. P.; Mirica, L. M. Unsupported d<sup>8</sup>-d<sup>8</sup> Interactions in Cationic Pd<sup>II</sup> and Pt<sup>II</sup> Complexes: Evidence for a Significant Metal-Metal Bonding Character. *Chem. Commun.* **2012**, *48*, 1532–1534.
- (40) Janiak, C. A critical account on  $\pi$ - $\pi$  stacking in metal complexes with aromatic nitrogen-containing ligands. *J. Chem. Soc., Dalton Trans.* **2000**, 3885–3896.
- (41) Moriguchi, T.; Kitamura, S.; Sakata, K.; Tsuge, A. Syntheses and Structures of Dichloropalladium(II)(Dithia[3.3]-Metadipyridinophane) and Dichloroplatinum(II)(Dithia[3.3]-Metadipyridinophane) Complexes. *Polyhedron* **2001**, *20*, 2315–2320.
- (42) de Graaf, W.; Boersma, J.; Smeets, W. J. J.; Spek, A. L.; van Koten, G. Dimethyl(N, N, N', N'-tetramethylethanediamine)-palladium(II) and dimethyl[1,2-bis(dimethylphosphino)ethane]-palladium(II): syntheses, x-ray crystal structures, and thermolysis, oxidative-addition and ligand-exchange reactions. *Organometallics* **1989**, *8*, 2907–2917.
- (43) Kim, Y.-J.; Jeon, H.-T.; Lee, K.-E.; Lee, S. W. Reactivity of the bis(silyl) palladium(II) complex toward organic isothiocyanates. *J. Organomet. Chem.* **2010**, *695*, 2258–2263.
- (44) Kundu, S.; Brennessel, W. W.; Jones, W. D. Synthesis and reactivity of new Ni, Pd, and Pt 2,6-bis(di-tert-butylphosphinito)-pyridine pincer complexes. *Inorg. Chem.* **2011**, *50*, 9443–9453.
- (45) See the [Supporting Information](#).
- (46) Fournier, É.; Lebrun, F.; Drouin, M.; Decken, A.; Harvey, P. D. Preparation and solid-state characterization of mixed-ligand coordination/organometallic oligomers and polymers of copper(I) and silver(I) using diphosphine and mono- and diisocyanide ligands. *Inorg. Chem.* **2004**, *43*, 3127–3135.
- (47) Allen, F. H.; Kennard, O.; Watson, D. G.; Brammer, L.; Orpen, A. G.; Taylor, R. Table of Bond Lengths determined by X-Ray and Neutron Diffraction. Part I Bond Lengths in Organic Compounds. *J. Chem. Soc., Perkin Trans. 2* **1987**, S1–S18.
- (48) Vicente, J.; Saura-Llamas, I.; Crünwald, C.; Alcaraz, C.; Jones, P. G.; Bautista, D. Palladium-assisted formation of carbon-carbon bonds. Part 10. Insertion reactions of isocyanides into the Pd-C bond of orthopalladated primary amines. Synthesis of 2-R-aminoisoidolinium salts (R = tBu, 2,6-Xylyl). *Organometallics* **2002**, *21*, 3587–3595.
- (49) Imhof, W.; Görls, H.; Halbauer, K. Tris(tert-butyl isocyanide-C)carbonyl-nickel(0). *Acta Crystallogr., Sect. E: Struct. Rep. Online* **2008**, *E64*, No. m1000.
- (50) Srinivas, V.; Balaraman, E.; Sajna, K. V.; Swamy, K. C. K. Catalyst-free and catalysed addition of P(O)-H bonds to allenyl/alkynyl-phosphonates and -phosphane oxides: Use of a robust, recoverable dinuclear palladium(I) catalyst. *Eur. J. Org. Chem.* **2011**, *2011*, 4222–4230.
- (51) Budzelaar, P. H. M.; Van Leeuwen, P. W. N. M.; Roobeek, C. F.; Orpen, A. G. [(dppe)Pd]<sub>2</sub>(SO<sub>3</sub>CF<sub>3</sub>)<sub>2</sub>: A palladium(I) dimer with “side-on” phosphine coordination. *Organometallics* **1992**, *11*, 23–25.
- (52) Khusnutdinova, J. R.; Rath, N. P.; Mirica, L. M. The Conformational Flexibility of the Tetradentate Ligand <sup>t</sup>Bu<sub>4</sub>N<sub>4</sub> is Essential for the Stabilization of (<sup>t</sup>Bu<sub>4</sub>N<sub>4</sub>)Pd<sup>III</sup> Complexes. *Inorg. Chem.* **2014**, *53*, 13112–13129.
- (53) Nelson, R. C.; Miller, J. T. An introduction to X-ray absorption spectroscopy and its in situ application to organometallic compounds and homogeneous catalysts. *Catal. Sci. Technol.* **2012**, *2*, 461–470.
- (54) Duan, H.; Li, M. H.; Zhang, G. H.; Gallagher, J. R.; Huang, Z. L.; Sun, Y.; Luo, Z.; Chen, H. Z.; Miller, J. T.; Zou, R. Q.; Lei, A. W.; Zhao, Y. L. Single-Site Palladium(II) Catalyst for Oxidative Heck Reaction: Catalytic Performance and Kinetic Investigations. *ACS Catal.* **2015**, *5*, 3752–3759.
- (55) Murahashi, T.; Nagai, T.; Okuno, T.; Matsutani, T.; Kurosawa, H. Synthesis and ligand substitution reactions of a homoleptic acetonitrile dipalladium(I) complex. *Chem. Commun.* **2000**, 1689–1690.
- (56) Constable, E. C.; King, A. C.; Raithby, P. R. Synthesis, coordination chemistry and crystal structures of [2 + 2] macrocycles incorporating 2,2-bis(thiomethyl)pyridine sub-units. *Polyhedron* **1998**, *17*, 4275–4289.
- (57) Che, C. M.; Li, Z. Y.; Wong, K. Y.; Poon, C. K.; Mak, T. C. W.; Peng, S. M. A simple synthetic route to N, N'-dialkyl-2,11-diaza[3.3](2,6)pyridinophanes. Crystal structures of N, N'-di-tert-butyl-2,11-diaza[3.3](2,6)pyridinophane and its copper(II) complex. *Polyhedron* **1994**, *13*, 771–6.
- (58) Connelly, N. G.; Geiger, W. E. Chemical Redox Agents for Organometallic Chemistry. *Chem. Rev.* **1996**, *96*, 877–910.
- (59) Frisch, M. J.; Trucks, G. W.; Schlegel, H. B.; Scuseria, G. E.; Robb, M. A.; Cheeseman, J. R.; Scalmani, G.; Barone, V.; Mennucci, B.; Petersson, G. A.; Nakatsuji, H.; Caricato, M.; Li, X.; Hratchian, H. P.; Izmaylov, A. F.; Bloino, J.; Zheng, G.; Sonnenberg, J. L.; Hada, M.; Ehara, M.; Toyota, K.; Fukuda, R.; Hasegawa, J.; Ishida, M.; Nakajima, T.; Honda, Y.; Kitao, O.; Nakai, H.; Vreven, T.; Montgomery, J. A., Jr.; Peralta, J. E.; Ogliaro, F.; Bearpark, M.; Heyd, J. J.; Brothers, E.; Kudin, K. N.; Staroverov, V. N.; Kobayashi, R.; Normand, J.; Raghavachari, K.; Rendell, A.; Burant, J. C.; Iyengar, S. S.; Tomasi, J.; Cossi, M.; Rega, N.; Millam, J. M.; Klene, M.; Knox, J. E.; Cross, J. B.; Bakken, V.; Adamo, C.; Jaramillo, J.; Gomperts, R.; Stratmann, R. E.; Yazyev, O.; Austin, A. J.; Cammi, R.; Pomelli, C.; Ochterski, J. W.; Martin, R. L.; Morokuma, K.; Zakrzewski, V. G.; Voth, G. A.; Salvador, P.; Dannenberg, J. J.; Dapprich, S.; Daniels, A. D.; Farkas, O.; Foresman, J. B.; Ortiz, J. V.; Cioslowski, J.; Fox, D. J. *Gaussian 09*, Revision A.02; Gaussian, Inc.: Wallingford, CT, 2009.
- (60) Becke, A. D. A New Mixing of Hartree-Fock and Local Density-Functional Theories. *J. Chem. Phys.* **1993**, *98*, 1372–1377.
- (61) Lee, C. T.; Yang, W. T.; Parr, R. G. Development of the Colle-Salvetti Correlation-Energy Formula into a Functional of the Electron-Density. *Phys. Rev. B: Condens. Matter Mater. Phys.* **1988**, *37*, 785–789.
- (62) Stevens, W. J.; Basch, H.; Krauss, M. Compact Effective Potentials and Efficient Shared-Exponent Basis-Sets for the 1st-row and 2nd-row Atoms. *J. Chem. Phys.* **1984**, *81*, 6026–6033.
- (63) Stevens, W. J.; Krauss, M.; Basch, H.; Jasien, P. G. Relativistic Compact Effective Potentials and Efficient, Shared-Exponent Basis-Sets for the 3rd-row, 4th-row, and 5th-row Atoms. *Can. J. Chem.* **1992**, *70*, 612–630.

(64) Hay, P. J.; Wadt, W. R. Ab initio effective core potentials for molecular calculations - potentials for the transition-metal atoms Sc to Hg. *J. Chem. Phys.* **1985**, *82*, 270–283.

(65) Hay, P. J.; Wadt, W. R. Ab initio effective core potentials for molecular calculations - potentials for K to Au including the outermost core orbitals. *J. Chem. Phys.* **1985**, *82*, 299–310.

(66) Foley, N. A.; Lail, M.; Lee, J. P.; Gunnoe, T. B.; Cundari, T. R.; Petersen, J. L. Comparative reactivity of TpRu(L)(NCMe)Ph (L = CO or PMe<sub>3</sub>): Impact of ancillary ligand L on activation of carbon-hydrogen bonds including catalytic hydroarylation and hydrovinylation/oligomerization of ethylene. *J. Am. Chem. Soc.* **2007**, *129*, 6765–6781.

(67) Veige, A. S.; Slaughter, L. M.; Wolczanski, P. T.; Matsunaga, N.; Decker, S. A.; Cundari, T. R. Deoxygenations of (silox)<sub>3</sub>WNO and R<sub>3</sub>PO by (silox)<sub>3</sub>M (M = V, Ta) and (silox)<sub>3</sub>NbL (silox = (Bu<sub>3</sub>SiO)-Bu-t): Consequences of electronic effects. *J. Am. Chem. Soc.* **2001**, *123*, 6419–6420.

(68) Chemissian, version 4.60, 2018, [www.chemissian.com](http://www.chemissian.com), accessed June 2019.

(69) O'Boyle, N. M.; Tenderholt, A. L.; Langner, K. M. cclib: A library for package-independent computational chemistry algorithms. *J. Comput. Chem.* **2008**, *29*, 839–845.

(70) Bruker Analytical X-Ray, Madison, WI, 2010.